

Discriminating the progenitor population of long and short GRBs

R. Coulman

University of Bath, Department of Physics, Bath BA2 7AY, United Kingdom
e-mail: rc2122@bath.ac.uk

Dated May 1, 2024

ABSTRACT

The recent detection of the long-duration, merger originating GRB211211A and GRB230307A has sparked a renewed interest in means to discriminate the progenitor population of GRBs based on their gamma-ray light curve alone. Traditional classification schemes, reliant solely on temporal and spectral properties to group GRBs into long and short bursts associated with stellar collapse and compact binary mergers, respectively, have proven inadequate in accurately discerning these anomalous GRBs. Building upon previous work, we utilise Haar wavelets to measure the variability of the bulk emission and systematically apply the technique in a novel manner to pulses preceding the main event, termed precursors. We find the former analysis of the prompt emission unable to disseminate the anomalous population, whereas the latter study of precursors correctly demonstrates clustering of the anomalies with the short merger population. Therefore, by utilising precursors, our work aids in the accurate classification of GRBs, which is essential for leveraging these bursts to understand star formation, metal enrichment, and the universe's evolution.

1. Introduction

Gamma ray bursts (GRBs) are the most energetic events in the observable universe, releasing jet collimated energies in excess of 10^{50} erg over timescales on the order of seconds (Kulkarni et al., 1999; Mészáros and Rees, 1999). Since their accidental discovery in the late 1960s (Klebesadel, Strong, and Olson, 1973) from gamma-ray detecting satellites designed to monitor nuclear testing by the Soviet Union, evidence has accrued for two primary modes of origin. GRBs are believed to either be produced from the gravitational collapse of massive stars, hereafter referred to as collapsars, or arise from the coalescence of compact binary systems comprising neutron stars and/or black holes. Both power the ejection of relativistic jets from either pole, that result in the gamma-ray emission observed.

Elucidation of the progenitor source of GRBs commonly relies upon the simple observational parameters T_{90} and the hardness ratio. In Kouveliotou et al.'s (1993) seminal paper, the T_{90} is defined as the duration encompassing 90% of the total GRB fluence, during which the cumulative flux increases from 5% to 95% above background. This quantity has proven an essential measure for classifying GRBs into long (> 2 s) and short (< 2 s) duration events; the former typically associated with collapsars and the latter with compact binary mergers (CBM). The T_{90} is connected with the spectral hardness ratio, a measure of the ratio of flux in high energy gamma ray bands to low energy bands. Short GRBs tend to exhibit a greater hardness ratio and are subsequently referred to as possessing harder spectra compared to their softer, long-duration counterparts (Kouveliotou et al., 1993).

While these parameters have provided a useful framework for discerning the progenitor source, two recent GRB detections have brought renewed challenges to the validity of the T_{90} and

hardness-ratio as means of classification. The 51 second long, spectrally soft GRB211211A had an associated kilonova, the radioactive glow of heavy elements formed in neutron star mergers, and other indications of its CBM origin, including zero spectral lag and a large offset from its host galaxy (Rastinejad et al., 2022). In parallel, GRB230307A, the second brightest GRB observed, displayed similar anomalous characteristics, including spectroscopic emission lines associated with tellurium (atomic mass $A = 130$), as detected by the James Webb Space Telescope (A.J. Levan et al., 2023). This discovery contrasts its 31 second duration and spectral softness. Pressingly, these GRBs bring to light widespread implications for previously classified GRBs, with Von Kienlin et al. (2020) suggesting that up to 10% of long GRBs at the peak of the T_{90} distribution may originate from CBMs, indicating a need to revise current theoretical models and classification techniques. Understanding the origin of GRBs is vital for gaining insights into stellar evolution, black hole formation, and the universe's early epochs. It is therefore of great importance to correctly discern progenitor populations so that one may use the appropriate GRB sample when studying phenomena like star formation or heavy element creation.

Simultaneously an interest has been growing in precursor events (e.g., Murakami et al., 1991; Ramirez-Ruiz, MacFadyen, and Lazzati, 2002; Lazzati, 2005; Neill et al., 2022), faint bursts of gamma-rays preceding the prompt emission by milliseconds to minutes. Despite their rarity, precursors may offer valuable insights into the underlying mechanisms of GRB progenitors and their emission process.

A strand of recent approaches (e.g., Beloborodov, Stern, and Svensson, 2000; Kocevski, Butler, and Bloom, 2007; Golkhou, Butler, and Littlejohns, 2015; Camisasca et al., 2023) have focused their efforts on analysing the variability of flux across mi-

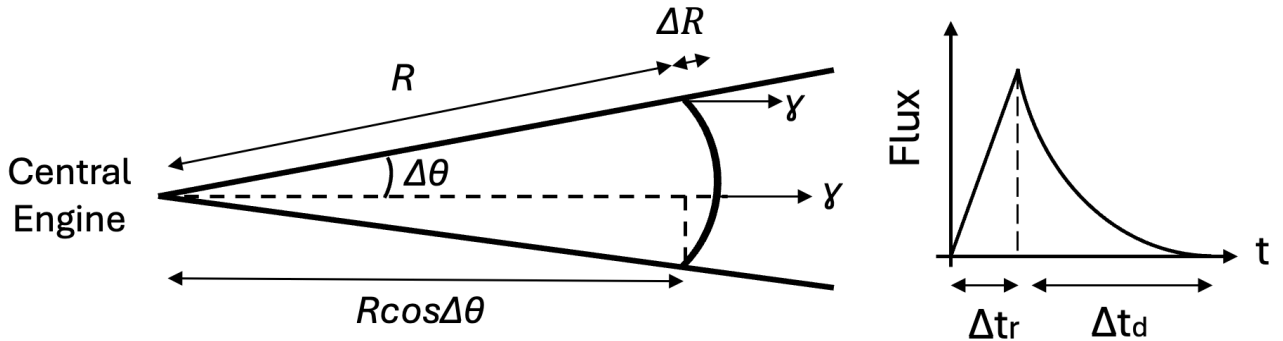


Fig. 1. The schematic illustrates a relativistic jet (left diagram) emitted from a central engine, typically a black hole, with a half-angle opening of $\Delta\theta$. Gamma radiation is emitted from the merged shell of thickness ΔR at a distance R . The right-hand side depicts a typical Fast Rise Exponential Decay (FRED) pulse resulting from this process.

cro and macroscopic timescales during the T_{90} . A review of the early progress made in this field has been performed by Golkhou and Butler (2014). A more recent investigation by Camisasca et al. (2023) found that the anomalous population of short GRBs with an extended T_{90} typically exhibit a variability timescale more appropriate of other merger originating bursts. However, the distinction is rather blurred and does not provide an infallible means of discrimination. In this report, we aim to expand upon previously established work in the study of variability within the T_{90} prompt emission, and apply these methodologies in a novel manner to precursor flares.

2. Expected differences between collapsars and CBMs

2.1. Fireball model

Examining anticipated differences between collapsars and CBMs within the fireball model posits how temporal variability may distinguish these progenitors. Both phenomena culminate in the formation of a black hole briefly surrounded by an infalling accretion disk of swirling hot debris, powering the ejection of two relativistic jets at the rotational axis of the remnant celestial body. The outflow of these jets is comprised of multiple shells with differing Lorentz factors Γ that expand and propagate adiabatically until a faster shell collides with a slower one. This facilitates the conversion of a significant fraction of their kinetic energy into radiation, predominately through synchrotron emission and inverse Compton scattering. Colliding internal shocks are responsible for the prompt emission observed in the γ -ray light curve. Subsequently, the remnant jet runs into the interstellar medium and results in a slower decaying afterglow that predominates in the lower energy regime.

Assuming the internal shock-wave shells have similar Lorentz factors, photons emitted at the front of the merged shell will reach the observer at a time roughly $\Delta R/c$ before those emitted at the rear. Here, c represents the speed of light, and the width of the merged shell, denoted by ΔR , dictates the rise time Δt_r of the pulse within the light curve. A more rigorous analysis must account for the highly relativistic nature of the shells, therefore, as Mészáros and Rees (1994) illustrate, any emission activity will appear to an external observer to be compressed in time by a factor of $1/2\Gamma_m^2$, where Γ_m is the Lorentz factor of the merged

shell. This yields a rise time of,

$$\Delta t_r \approx \frac{\Delta R}{2c\Gamma_m^2}. \quad (1)$$

In practice, the excited baryonic matter continues emitting radiation post-collision during a finite cooling period, but this timescale is negligible compared to the duration of the shells intersection (Piran, 2005). The decay time Δt_d of the pulse is instead governed by angular effects, with the detection of off-axis emission being delayed in proportion to the radius R of the colliding shells from the central engine. The precise relationship,

$$\Delta t_d = \frac{R(1 - \cos \Delta\theta)}{c} \approx \frac{R(\Delta\theta)^2}{2c} \approx \frac{R}{2c\Gamma^2}, \quad (2)$$

falls from simple geometric arguments as depicted in Figure 1, where $\Delta\theta$ is the half angle opening of the jet. Due to the near light speed velocities of the propagating shells, this angle is beamed into $\Delta\theta \sim \Gamma^{-1}$ (Kocevski, Butler, and Bloom, 2007). The prompt emission of a GRB is primarily attributed to the culmination of internal shocks, which results in a superposition of experimentally determined fast rise, exponential decay (FRED) pulses, originating from individual shock-wave collisions. This characteristic profile is depicted later in Figure 2. Short GRBs on average release less total energy than longs (e.g., Ghirlanda et al., 2009; D’Avanzo, 2015), and have a more constrained upper bound on the size of the central engine (Barnacka and Loeb, 2014; Golkhou and Butler, 2014). Therefore, the absolute value of $\langle \Gamma \rangle$ should be lower for shorts (Nakar, 2007; Matsumoto and Piran, 2020), leading to an earlier collision of the shells, at a smaller radius, assuming a similar relative distribution of velocities. Importantly, this insinuates a subtle expected difference in the rise and decay time between the two progenitors. However, the bulk parameters, including the T_{90} and hardness ratio, are unlikely to pick up on such intricacies.

Despite the success of the internal shock model in accounting for the short timescale variability of GRBs, it is worth noting that it faces challenges explaining the spectral index below the peak energy, as well as the low efficiency ($\sim 20\%$) of kinetic energy conversion to γ -rays (Kumar and Zhang, 2015). Following the main γ -ray emission, the remaining kinetic energy of the relativistic jet runs into the interstellar medium, heating it, producing

a slower decaying, softer afterglow described by the external shock scenario (e.g., Pe’Er et al. (2015)).

2.2. Precursors

Precursors are defined as a relatively dim pulse of γ -rays observed prior to the main burst, and are thought to originate from distinct physical processes. The fraction of long-duration GRBs with precursors is believed to lie between 3% and 20%, whereas the fraction of short bursts possessing precursors falls between 1% and 3% (Zhong et al., 2019; Coppin, Vries, and Eijndhoven, 2020), depending upon the precise definition. Several models have been proposed to explain their origin; however, a widely accepted framework remains elusive. A prominent theory for collapsar precursors proposes that shortly after the gravitational collapse of the stars core, the initial jet breaks through the outer stellar mantle, generating a precursor upon the shock’s breakout (Ramirez-Ruiz, MacFadyen, and Lazzati, 2002). This process can occur many seconds before the collision of internal shocks, believed to cause the main prompt emission. Conversely,Neill et al. (2022) posit that merger precursors instead originate from resonant shattering flares (RSFs)—bursts of γ -rays triggered by tidal resonance of a neutron star during binary inspiral. As the orbital frequency approaches the natural frequency of one of the oscillatory modes within the neutron star, resonant excitation of that mode may occur, leading to faults in the star’s crust and potentially RSFs.

Despite the uncertainty surrounding the origin of precursors, their presence makes them an interesting parameter as a potential diagnostic tool. Especially considering the vastly different mechanisms predicted to produce precursors in collapsars and CBMs, potentially resulting in greater differences between their light curves compared to those of the main prompt emission.

3. Data set

We primarily focus on GRBs detected with *Swift*/BAT, occasionally including those from the *Fermi* Gamma-ray telescope in cases where the former has not detected the burst or did so with a low signal-to-noise (SNR) ratio. For GRBs detected with *Swift*, we use the calibration files from the 2023-06-07 BAT database release to establish the energy scale and mask weighting for the BAT data. The mask weighting procedure is employed to derive background subtracted light curves. We then construct 1 ms binned light curves in the 15-150 keV energy range. This entire process is performed using the *Swift* tools BATHTOPIX, BAT-MASKWTEVT, and BATBINEVT from the HEASoft 6.33 software release. My supervisor, Patricia Schady, wrote a program to automate this pipeline.

Schady also downloaded Fermi data from the online *Fermi*/GBM trigger catalogue¹. From the 12 sodium iodide scintillators we selected the light curve that exhibited the most visually prominent GRB. Unless specified otherwise, we primarily extracted 16 ms binned light curves in the 8-900 keV energy range, noting that *Fermi* allows for analysis of a greater energy range. A polynomial is fitted to the background to yield a background subtracted light curve.

¹ <https://heasarc.gsfc.nasa.gov/W3Browse/fermi/fermigtrig.html>

After processing the data, we analysed specific samples of GRBs that broadly fit into three categories. A subset consisting of eight short GRBs, classified on their T_{90} , with precursors were examined. This comprises four *Swift* GRBs with precursors identified by Troja, Rosswog, and Gehrels (2010), and four GRBs observed with *Fermi* as detailed by Coppin, Vries, and Eijndhoven (2020). The latter paper also classifies a further 27 long *Swift* GRBs with precursors, which we use as our first sample together with the short bursts containing precursors.

From previous stipulations, it is possible that some of these GRBs classified purely by their duration may not be produced by their traditionally espoused source. To this extent, we analyse 14 *Swift* GRBs with an associated supernova (SN), as determined by Cano, Wangand Dai, Wu, et al. (2017), ensuring to only select SNe graded A-C. Grade A signifies a spectral classification of the SN, delineating its highly probable collapsar origin, while grade C indicates an afterglow consistent with an SN. We also examine 2 short bursts, GRB130603B (Tanvir et al., 2013) and GRB160821B (Troja, Castro-Tirado, et al., 2019), with an associated kilonova (KN), along with the famed GRB170817A with gravitational wave detection (Abbott et al., 2017).

The final sample contains the anomalous, kilonova associated *Swift* GRB211211A and *Fermi* GRB230307A. The former pertains a possible short precursor (Zhou et al., 2024), along with the latter (Dichiara et al., 2023), although, eminent in the 8-100 keV energy range, promoting our analysis in this domain. Other less prominent GRBs have also been identified as anomalous, including GRB060614 (e.g., Caito et al., 2009; Yang et al., 2015), and GRB211227A (e.g., Lü et al., 2022; Ferro et al., 2023), both of which we utilise in our final sample. The light curves of the four anomalous GRBs are available in the Appendix.

The T_{90} durations, along with their associated errors, are obtained online from NASA’s GRB database². The precursor durations, T_{pre} , are instead gathered from the cited papers above and have typically been obtained using a Bayesian block analysis, although no uncertainties are provided. Future investigations may therefore gain slight benefit from calculating the T_{90} of the precursor duration to obtain an appropriate error. This would also offer a fairer comparison between the precursor duration and T_{90} of the prompt emission. Achieving this entails using the times reported in the cited papers as an initial reference point.

Despite this, the detailed sample of GRBs with precursors, supernova and kilonova, and mergers with anomalous T_{90} , allows for the validation of data analysis techniques on bursts with a known progenitor source. Through this, we can ascertain if there is a measurable difference between the light curves of long and short GRBs classified by their T_{90} , and those with SN or KN detection. After validating the method and comparing the results to established studies we can then apply the technique to the lesser investigated precursors.

4. Data analysis

4.1. Spectral analysis

My project partner explored the γ -ray spectrum of GRBs as a function of counts across energy bins. The data follow a power-law or cutoff power-law model, exhibiting decreasing counts at

² https://swift.gsfc.nasa.gov/archive/grb_table/

higher energy ranges. This behavior derives from the synchrotron emission spectrum, the predominant emission process within the internal shock model. The γ -ray spectrum of synchrotron radiation, characterized by its frequency f , from an electron, exhibits two distinct power-law segments connected by a kink. Within the high-energy domain the power spectrum exhibits an initial decline of approximately $f^{-1/2}$, succeeded by a faster decay in a region of rapid cooling (Piran, Narayan, et al., 1998). This power-law emission pattern is reflected in the energy spectrum of GRBs, with the break energy between the two segments typically exceeding 150 keV, the maximum range of *Swift*.

The longer-duration prompt emission fits are evaluated using a reduced chi-squared test, whereas for the typically shorter-duration precursors with fewer counts per bin, we use the better suited Cash statistic. This latter step is essential as the reduced chi-squared test necessitates a minimum of 20 counts per bin for reliable analysis, a criterion not met by all precursor durations. Both the fits and uncertainties are determined using XSPEC 12.14. The Akaike Information Criterion (AIC) is then employed to determine the best fit between the power-law and cutoff power-law model. As *Swift* BAT has a narrow energy range it typically favours a single power-law, while a cutoff power-law often better fits *Fermi* data which is sensitive into the energy range of 900 keV, far beyond the typical break.

Subsequently, we measure the photon index—a measure of the gradient of the logarithmic spectrum of photon counts across energy bins. Since short GRBs are generally harder, we expect a greater relative photon count at higher energies than their long-duration counterparts, leading to a flatter gradient and smaller subsequent photon index. The purpose of this analysis is to evaluate a measure of spectral hardness for the precursors within our sample. The photon index should provide a more accurate way to do so, provided a sufficient SNR, as it offers a more nuanced measurement compared to a simple ratio of high to low energy counts.

4.2. Variability analysis

As Daigne and Mochkovitch (2003) notes, and as one would expect from the internal shock model, the complex variability of the GRB light curve (LC) likely directly corresponds to the activity of the central engine, and thus suitable analysis of the LC may aid in discerning the progenitor source. Several approaches have previously been adopted to measure such variability, including the structure function (SF) (Trevese et al., 1994), auto-correlation function (ACF) (Link, Epstein, and Priedhorsky, 1993), and Fourier power spectral density (PSD) (Beloborodov, Stern, and Svensson, 2000). In this paper, we instead build on the work of Kocevski, Butler, and Bloom (2007), opting to use Haar wavelets for their propensity to describe narrow time features (Kolaczyk, 1997). This avoids the Gibbs phenomenon associated with the PSD, and its Fourier transform the ACF, when characterising sharp discontinuities promiscuous in GRB light curves. Work by Golkhou and Butler (2014) has also linked the Haar wavelet scaleogram to previous analysis utilising SFs.

In their simplest Haar wavelets $h_{i,\Delta t}$ measure the extent to which the average count rate over a timescale Δt changes from one interval to the next. The initial calculation averages the natural logarithm of the count rate over Δt consecutive bins X to

obtain an averaged bin,

$$\bar{X}_{i,\Delta t} = \frac{1}{\Delta t} \sum_{j=0}^{\Delta t-1} X_{i\Delta t+j}. \quad (3)$$

During the processing of GRB light curves, we used fixed binning, enabling the number of bins Δt to be expressed equivalently in terms of their corresponding time interval. Importantly, experimenting with LCs of different binning should minimally impact this process, as it merely alters the minimum width at which averaging commences. However, if one wishes to have greater sensitivity at more microscopic scales, they may be advised to initially bin the LC over a very fine duration.

The Haar wavelet coefficients,

$$h_{i,\Delta t} = \bar{X}_{2i+1,\Delta t} - \bar{X}_{2i,\Delta t}, \quad (4)$$

are then determined over non-overlapping intervals, representing the difference between two successive boxcar-averaged points. We form a Haar scaleogram,

$$\sigma_{\Delta t}^2 = \frac{\Delta t}{t} \sum_{i=0}^{t/2\Delta t-1} h_{i,\Delta t}^2, \quad (5)$$

also termed the Allan (1966) variance $\sigma_{\Delta t}$, by averaging the coefficients at each scale Δt , where t is the total number of bins within the original LC (Kocevski, Butler, and Bloom, 2007).

Most LCs exhibit a relatively low signal-to-noise ratio (SNR), and subsequently, at very short timescales, the difference between adjacent data points may be considered random, irrespective of the macroscopic behavior at that position. Namely, $h_{i,\Delta t}$ will, to a close approximation, be the same at flat and peaked regions of the LC over small Δt scales. For all but very high SNR LCs, we thus expect an initial fall in $\sigma_{\Delta t}$ as the magnitude of $h_{i,\Delta t}$ remains relatively constant while the number of coefficients decreases with enlarging averaging window size, at a rate greater than that offset by the normalisation factor $\Delta t/t$. As Δt increases and the averaging window widens, the light curve becomes smoother, and the macroscopic behavior begins to resolve, as illustrated in Figure 2. Correspondingly, $\sigma_{\Delta t}$ rises over the scale at which consecutive averaged bins are likely to only incorporate data from a single pulse, and is hence termed to be probing correlated variability. Previous studies (Walker, Schaefer, and Fenimore, 2000; MacLachlan et al., 2013) take the first instance above this minima to be physically meaningful, representing the minimum variable timescale (MVT) at which the LC surpasses the Poisson background noise. A plateau in $\sigma_{\Delta t}$ should manifest as Δt increases further, resulting in averaged bins that are more probable than not to contain elements from the rise and fall of a pulse, leading to destructive interference. This flattening of the gradient can be observed later in the right-hand panel of Figure 4, where over this scale, $\sigma_{\Delta t}$ is deemed to be measuring uncorrelated variability. In the extreme, the graph should turnover as Δt becomes on the order of t and the number of Haar coefficients greatly falls. Although in this report we are not concerned with this aspect. This analysis broadly agrees with Hughes, Aller, and Aller's (1992) work on the structure function.

Instead of taking the MVT as the first instant above the Poisson floor, Golkhou and Butler (2014) show this minima to only

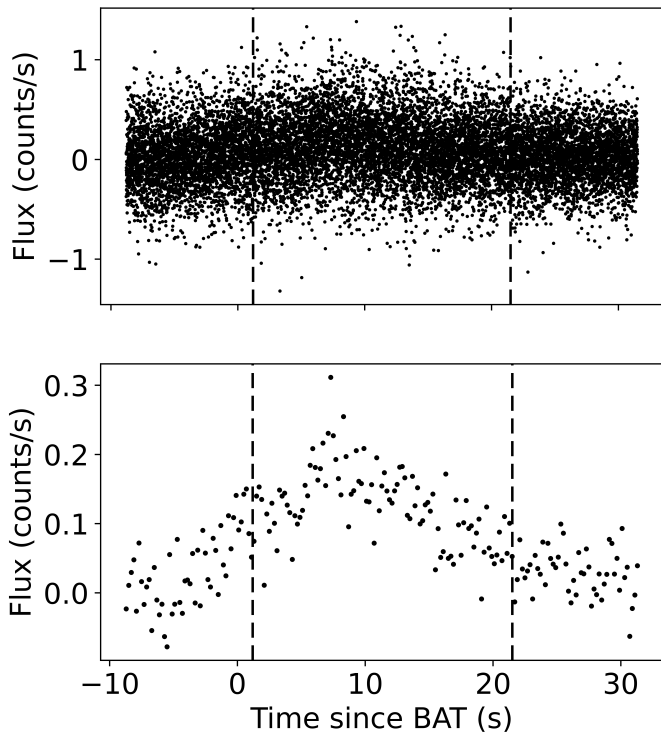


Fig. 2. The *Swift* γ-ray light curve of GRB120118B between the T_{90} (dashed lines) at 3 ms (top) and 200 ms (bottom) binning. This illustrates how the Allan variance $\sigma_{\Delta t}$ is insensitive to the macroscopic behaviour at small bin sizes, particularly under conditions of high noise.

track the background noise of the LC. They instead define a more physically meaningful scale for the MVT as the transition between (smooth) correlated and (unsmooth) uncorrelated variability, proposing it to more accurately tie in with time scales present in the GRB. They quantify this as the point at which, relative to the Poisson floor, $\sigma_{\Delta t}$ is no longer proportional to Δt . The main problem with this approach, however, is the ambiguity at which one defines the precise point within the minima to begin defining the linear behavior. Another challenge arises from the fact that in most real cases over this scale, $\sigma_{\Delta t}$ is best described by a polynomial. Therefore, fitting a straight line may not be the optimal method since its magnitude often relies on the accuracy with which you map the polynomial. These intrinsic issues can again be observed in the right-hand panel of Figure 4, which illustrates the typical behavior of $\sigma_{\Delta t}$. For these reasons, in this paper we instead adopt the approach of fitting an n^{th} order polynomial to the data and determining its first derivative's maximum between the Poisson floor and turnover to define the MVT. For a smoothly increasing $\sigma_{\Delta t}$, this coincides with the half maxima of the scaleogram. Equally, if $\sigma_{\Delta t}$ is jagged, it will only track the first smooth rise phase, in line with Golkhou and Butler's (2014) method. This technique, however, offers three main advantages: (1) the data are much better described over this range by a polynomial; (2) it doesn't require defining an initial starting point; (3) the method allows for greater automation with less intervention and bias.

The uncertainty in $\sigma_{\Delta t}$, propagated from detector count errors, is generally minimal. Consequently, the primary source of uncertainty in the MVT arises from uncertainties in the polynomial fit. Therefore, in subsequent plots, we omit the minor errors

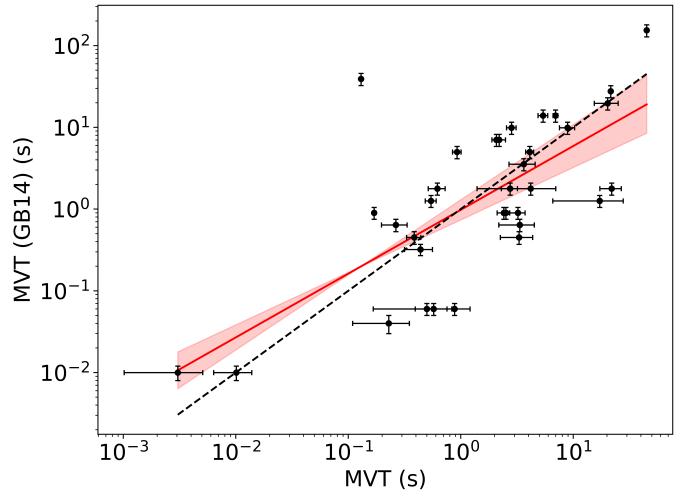


Fig. 3. Comparison between the MVT obtained by Golkhou and Butler (2014)—abbreviated to GB14 in the plot—with the MVT determined through the revised method introduced in this paper, utilising a random sample of shared *Swift* GRBs. In both cases, the uncertainties are derived from the fit of the model, as are they for all proceeding plots. The black dashed line corresponds to equality, while the solid red line of slope 0.78 ± 0.14 , and shaded area show the best fit and $1-\sigma$ region, respectively.

associated with $\sigma_{\Delta t}$. Instead, we calculate the uncertainty in the MVT as the mean difference between the best-fit MVT and that a polynomial fit a degree above and below.

It is worth exploring how the MVT obtained from our method compares to that of Golkhou and Butler (2014). To this aim, we selected a random sample of 34 BAT GRBs from those analysed in Golkhou and Butler's (2014) paper and computed the MVT of the bursts. Figure 3 shows this comparison, revealing a strong correlation about the equality (dashed-line), although not complete interchangeability. This offers a promising validation of our method, with the main difference stemming from how the transition from correlated to uncorrelated variability is measured.

4.3. Physical interpretation of the minimum variable timescale

There is some ambiguity as to the physical interpretation of the MVT, with a few suggestions (Golkhou and Butler, 2014, Veres et al., 2023) that it closely tracks the rise time of the smallest pulse within the LC. To evaluate this further, we have generated some simple FRED profiles typical of a GRB, as shown in Figure 4.

In keeping with Golkhou and Butler (2014), we find that a LC devoid of artificial noise initially exhibits a rise phase in $\sigma_{\Delta t}$ without a preceding decline, confirming that the first moment above the Poisson floor solely tracks the background noise. Contrary to the previous stipulation that the MVT solely tracks the rise time, however, the single pulse comprising a 4 s rise time is instead found to pose an MVT of (0.79 ± 0.16) s. An additional simulation with superimposed pulses, of respective rise time of 7 s and 5 s, and subsequent MVT of (1.21 ± 0.19) s, aids in confirming this disparity between the rise time and MVT. The slight discrepancy between our method and that used previously is likely not large enough to account for this difference. Thus, we conclude in conjunction with Camisasca et al. (2023) that while

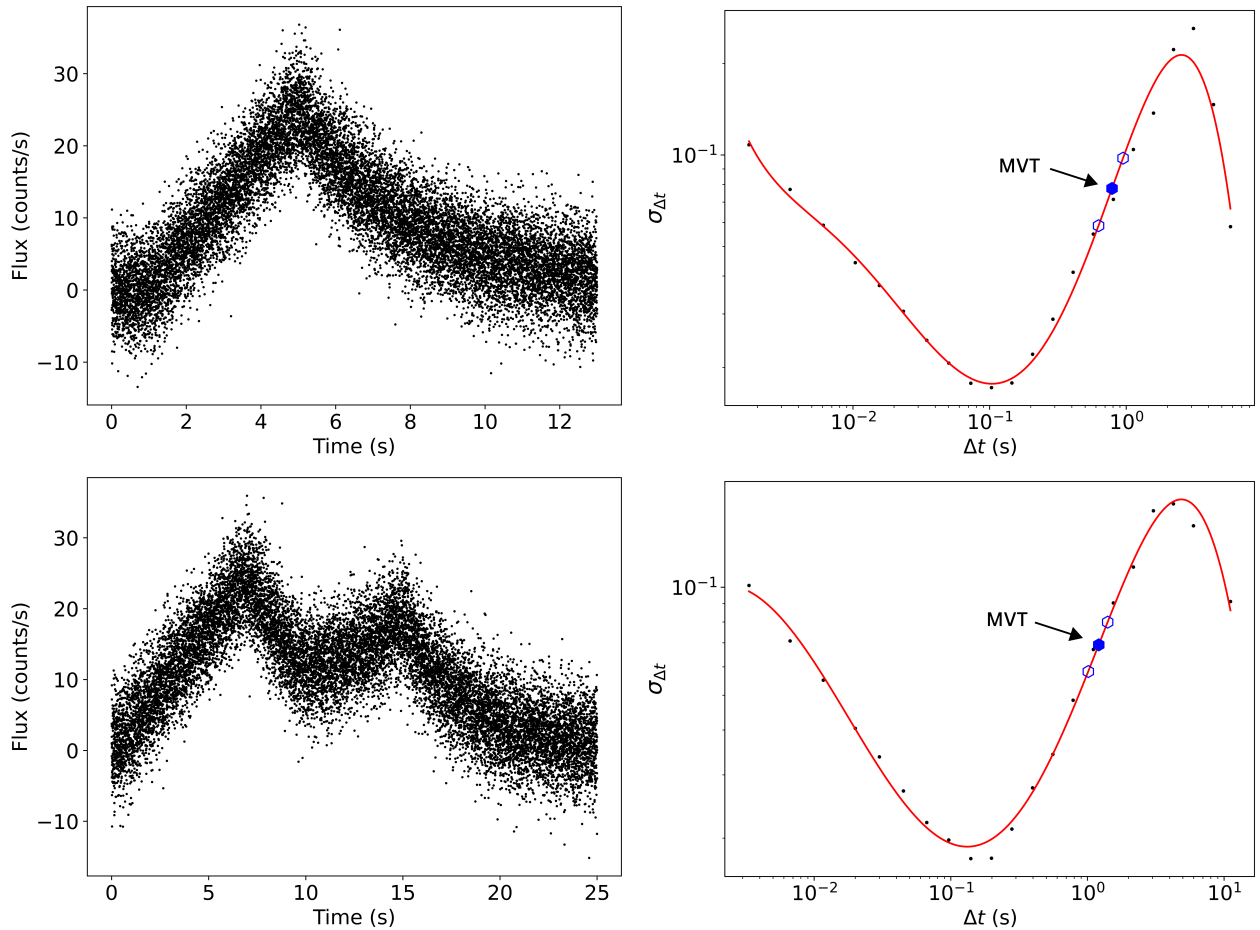


Fig. 4. (Top) A simulated FRED pulse with a rise time of 4 s, proceeding a 1 s delay, and (Below) two superimposing pulses with a respective rise time of 7 s and 5 s. The MVT (filled blue hexagon) for the first LC is (0.79 ± 0.16) s, while the second is (1.21 ± 0.19) s, neither of which correspond with the rise time. As the plots are artificially generated, there are no uncertainties to propagate in the Allan variance $\sigma_{\Delta t}$, although the MVT of a polynomial degree above and below is illustrated (hollow blue hexagons).

sometimes simple connections are found between the MVT and properties such as the rise time, the interpretation is typically less straightforward.

But while the MVT doesn't explicitly return the rise time, it may still vary in proportion to it, along with other parameters. In Figure 5, we investigate this hypothesis, evaluating the relationship between the MVT and the rise time (s), decay time (s), full width at half maximum (FWHM) (s), and amplitude coefficient for a single pulse. The period analysed initiates 1 s prior to the rise time and ceases when the decay is valued at 10% of the pulses peak. While one parameter is varied, the others are held constant at a rise and decay time of 3 s, variable FWHM, and an amplitude coefficient of 15. The MVT of increasing rise and decay time (shown as an orange circle and teal square respectively) exhibits initial growth followed by a plateau as the variable element no longer dominates the LC. A stronger relationship is witnessed between the MVT and FWHM (depicted as a beige triangle), likely reflecting the concurrent enlargement of rise and decay times. This dependency is supported by the recent work of Camisasca et al. (2023), who established a robust correlation between the MVT, determined by Golkhou and Butler (2014), and the FWHM of the smallest statistically significant peak within the LC. If typical pulses were liner-symmetric then the FWHM would be equivalent to the rise time, however, as

most are instead more aptly described by a FRED profile, these two parameters are not interchangeable. Although, this may help clarify why previous findings depict connections between the rise time and MVT. Additionally, the correlation with the FWHM would also help explain the juxtaposing effect on the MVT of increasing amplitude (illustrated as a purple diamond) over a fixed time domain, as this has the result of reducing the FWHM.

Crucially, while the MVT most closely tracks the FWHM, it does not do so in isolation, instead, we find it to exist in a multi-dimensional phase space with dependence on the four variables measured here, and likely more. A caveat of this analysis is that a simulated pulse may not be fully representative of a GRB LC, however, minor discrepancies are unlikely to alter the overarching conclusion. Further, the lack of a simple connection doesn't preclude an invalidation of the method, rather, it likely illustrates a more nuanced nature of the MVT that implores the temporal richness of a LC over many scales.

5. Results

5.1. Photon index

We commence our analysis examining the relationship between the T_{90} and photon index PI_{90} over this duration, as shown in Figure 6. We differentiate between short and long GRBs using

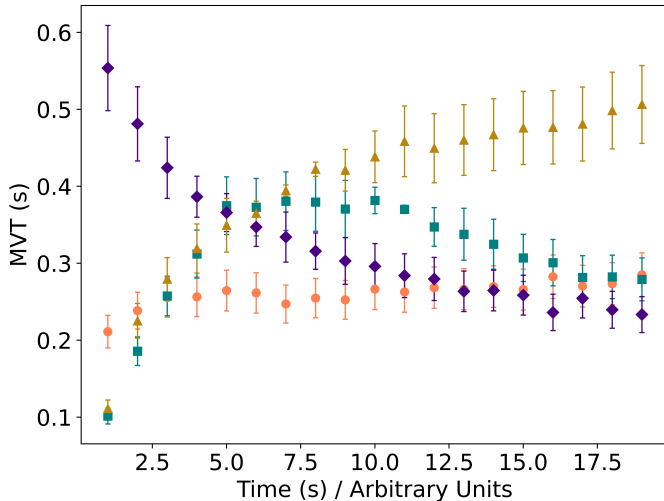


Fig. 5. MVT for a single simulated FRED pulse, illustrated in Figure 4, as a function of varying rise time (s) (orange-circle), decay time (s) (teal-square), full width half maxima (s) (beige-triangle), and amplitude coefficient (arbitrary units) (purple-diamond). In a given analysis, the other parameters are held constant at 3 s, 3 s, undefined, and 15, respectively. For all, the decay time is determined as the duration between the peak and 10% of the full maxima.

the colors red and blue, respectively, where hollow squares indicate a conformation of classification in the typical form of either a KN or SN. Conversely, green is reserved for the anomalous GRBs. While Figure 6 shows separation between the short and long populations, this is mainly evident in the 1-dimensional T_{90} domain. One interpretation of this observation is that the photon index may be less effective in capturing flux variation across energy bins in comparison to the hardness ratio. However, in contention, we note that the distinction observed in the hardness ratio is far more blurred in a significant number of cases (Tarnopolski, 2019). In general, the plot confers the expectation that short-duration bursts have a lower PI than long GRBs, and with a greater abundance of data, a more pronounced clustering along the diagonal may emerge.

A comparison between the precursor photon index PI_{pre} , and PI_{90} proves less enlightening due to unbounded uncertainties associated with the former. These originate from the very brief duration of some precursors, resulting in too few counts per energy bin to constrain the photon index accurately, despite implementation of the Cash statistic. Figure 7 is thus shown without error bars, revealing the best-fit distribution that, on average, illustrates a larger photon index in the prompt emission. This finding contradicts previous studies (Zhong et al., 2019, Lazzati, 2005) that found the precursor to be spectrally softer than the prompt emission. Consequently, we exclude further analysis of PI_{pre} as the uncertainties are too great to draw reliable conclusions.

5.2. Minimum variability timescale in T_{90} bursts

Here we begin by looking at a possible connection between the T_{90} minimum variability timescale MVT_{90} and the T_{90} duration over all samples noted in Section 3. However, to ensure integrity of the results, LCs that yielded ambiguous plots of the Allan variance $\sigma_{\Delta t}$ without a clear rise phase have been excluded. These typically proceeded from LCs with a low SNR and were more

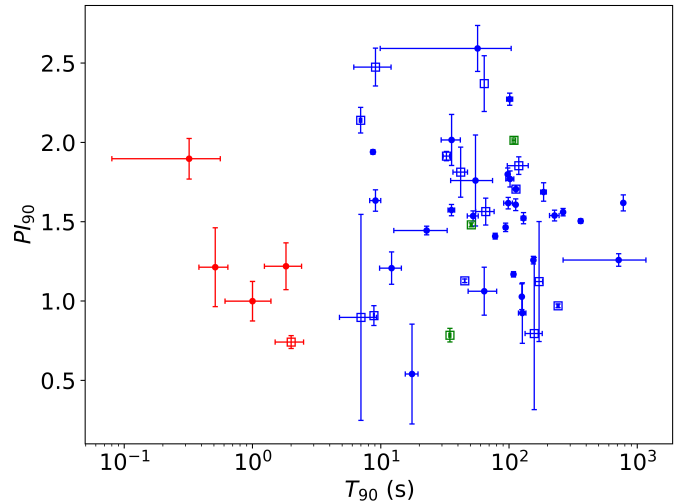


Fig. 6. Photon index PI_{90} plotted versus the T_{90} duration. Short duration bursts (< 2 s) are plotted in red, and long bursts (> 2 s) in blue, whereas green denotes GRBs of merger origin that pertain an extended T_{90} . Hollow squares are reserved for GRBs with an associated supernova or kilonova. This formatting is maintained for all subsequent plots. The uncertainties associated with the photon index reside from the reduced chi-squared test used during fitting of the power law model, Whereas the T_{90} uncertainties are taken directly from NASA's GRB database delineated, in Section 3.

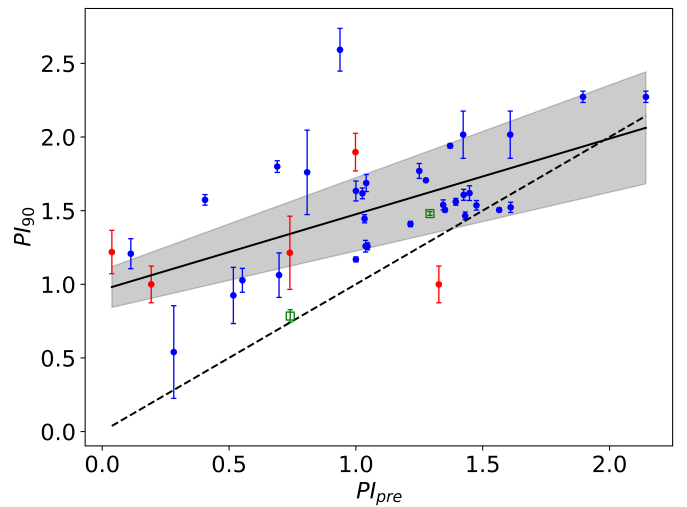


Fig. 7. The photon index over the T_{90} , PI_{90} and precursor duration, PI_{pre} . The solid line and shaded area illustrate the best fit and $1-\sigma$ region, as do they for all proceeding plots, while the dashed line denotes equality. The uncertainties of PI_{pre} are unconstrained, typically of magnitude 6, and have been removed to observe the most probable distribution, although it is noted to be highly inaccurate.

abundant in short GRBs, a trend attributed to the inherently lower volume of data. The findings are presented in Figure 8. A clear trend (Spearman's rank coefficient $\rho = 0.66$, $p < 10^{-11}$), defined by the slope 0.68 ± 0.07 , is seen between the T_{90} duration and the MVT of the LC spanning this domain. This correlation has been noted before (Golkhou and Butler, 2014, Veres et al., 2023), and here we pose that it stems partly from the intrinsic limit that the duration imposes on $\sigma_{\Delta t}$. The maximum timescale that Δt can possess for $\sigma_{\Delta t}$ to be non-zero is half the width of the duration. Any greater and the averaging window will be too

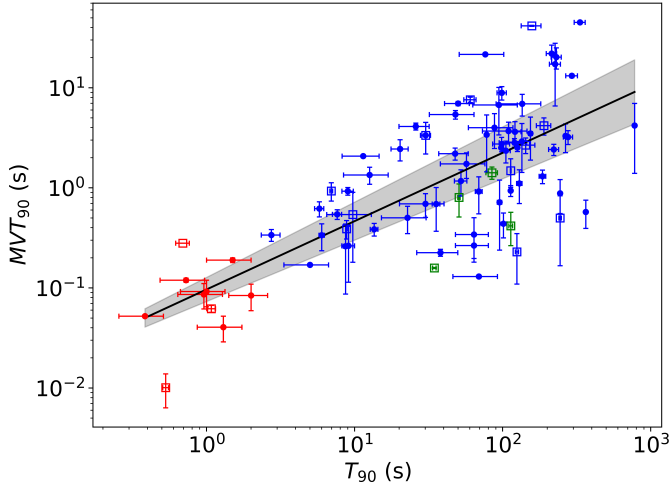


Fig. 8. The minimum variable timescale MVT_{90} against the T_{90} duration. The solid line of best fit has slope 0.68 ± 0.07 . The sample includes GRBs detailed in Section 3 and those analysed in Figure 3.

large to produce two discrete bins, resulting in an undefined Haar coefficient $h_{i,\Delta t}$. This necessarily means that the MVT is at least constrained by the duration, rather than solely the behaviour of pulses. This plot also depicts strong alignment between the temporally defined long and short bursts and those classified with associated SN, KN, or other multi-messenger modes. This is to be expected as only a small fraction of GRBs are believed to differ from their temporally classified source.

Less common in the literature are reviews of the MVT as a function of measures of spectral hardness, as shown in Figure 9. However, we find no statistically significant ($\rho = 0.21$, $p = 0.14$) correlation between the MVT_{90} and PI_{90} , and only a slight separation between the long and short populations. This in part originates from the weak correlation found in Figure 6.

5.3. Minimum variability timescale in precursors

In the previous figures, the anomalous GRBs are visually indistinguishable from the bulk of the long-duration bursts. We thus turn our attention to Figure 10, depicting the precursor minimum variability timescale MVT_{pre} against both the T_{90} and precursor duration, T_{pre} . We note that GRB090510 has two precursors, only one of which a reliable MVT could be extracted. Additionally, GRB060614 and GRB211227A are not featured in these plots despite having an initial emission period that falls to background before an extended burst, thus meeting one criteria of a precursor. However, this initial burst exhibits significantly greater peak fluence than the subsequent emission, therefore failing to meet the crucial condition that the precursor should be fainter than the prompt emission. These precursor flares may be observed in the Appendix. If CBM precursors indeed originate from RSFs or other resonance-related effects, then these bursts should be substantially less energetic than the main collision. Further, we also note that the sample of GRBs with an associated SN or KN lack precursors and so do not appear in plots featuring MVT_{pre} .

In line with earlier observations illustrated in Figure 8, the precursor and T_{90} duration in Figure 10 are highly correlated with MVT_{pre} ($\rho = 0.83$, $p < 10^{-7}$; $\rho = 0.59$, $p = 6 \times 10^{-4}$, respectively). We employ a rationale akin to the one previously outlined, which

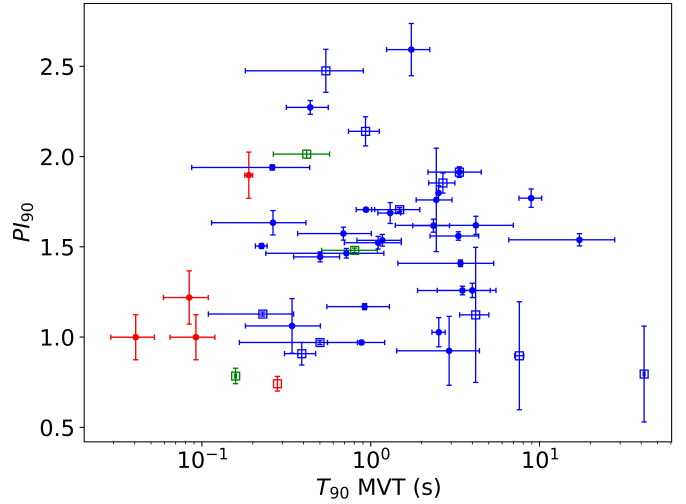


Fig. 9. The photon index PI_{90} plotted with the minimum variable timescale MVT_{90} , over the T_{90} duration.

explains the constraint imposed by the duration on the MVT, to help partially elucidate the former connection between T_{pre} and MVT_{pre} . Although a less trivial explanation may be needed to account for the latter relation between T_{90} and MVT_{pre} , and we delineate a possible interpretation in Section 6.2. Importantly, Figure 10 shows a far greater degree of separation between the anomalous and long GRBs, with tight clustering of the anomalies to the short-duration bursts in the left-hand plot.

One notable long-duration GRB161129A, with a T_{90} of (35.5 ± 2.1) s, also exhibits a close proximity to the short burst, along with the anomaly cluster. In the absence of an associated SN, one possible conclusion is that this burst originates from a CBM. If Von Kienlin et al.’s (2020) upper limit of a 10% misclassification rate amongst long GRBs holds true, then we should expect at least one of the 24 long-duration bursts within our sample to be attributable to a merger origin. To evaluate this possibility, we examined the lower energy *swift* X-ray LC and found resemblance of a rapid decay proposed by Gompertz et al. (2013) to be a signature of CBMs. Furthermore, examining the spatial localisation of the GRB161129A reveals that within the uncertainty radius of its position, the burst was situated close to two galaxies separated by 1.4 arcseconds (Heintz et al., 2021, GCN Circ. 20244). The GRB is suggested (Cano, Malesani, et al., 2021, GCN Circ. 20245) to originate from the galaxy with which it exhibits a lower offset, on the premise it was produced from a collapsar. Conversely, large offsets from host galaxies are typical of merger origin, as the supernova associated with the genesis of a neutron star imparts large velocities, ejecting the neutron star from its birthplace. Therefore, if GRB161129A were produced from a CBM, then a large offset is expected, instead suggesting the galaxy with a greater separation may be the host. However, in the absence of any strong evidence, an equally plausible interpretation is that the associated GRB may simply reside at the lower tail of the MVT_{pre} distribution of collapsar originating bursts.

To this extent, we compare MVT_{pre} to MVT_{90} in Figure 11 and find a slight displacement in GRB161129A’s (highlighted in purple) clustering from the short and anomaly groups compared to Figure 10. Assuming that the MVT_{pre} distribution found thus far is reflective of a larger sample of GRBs, and that long-duration

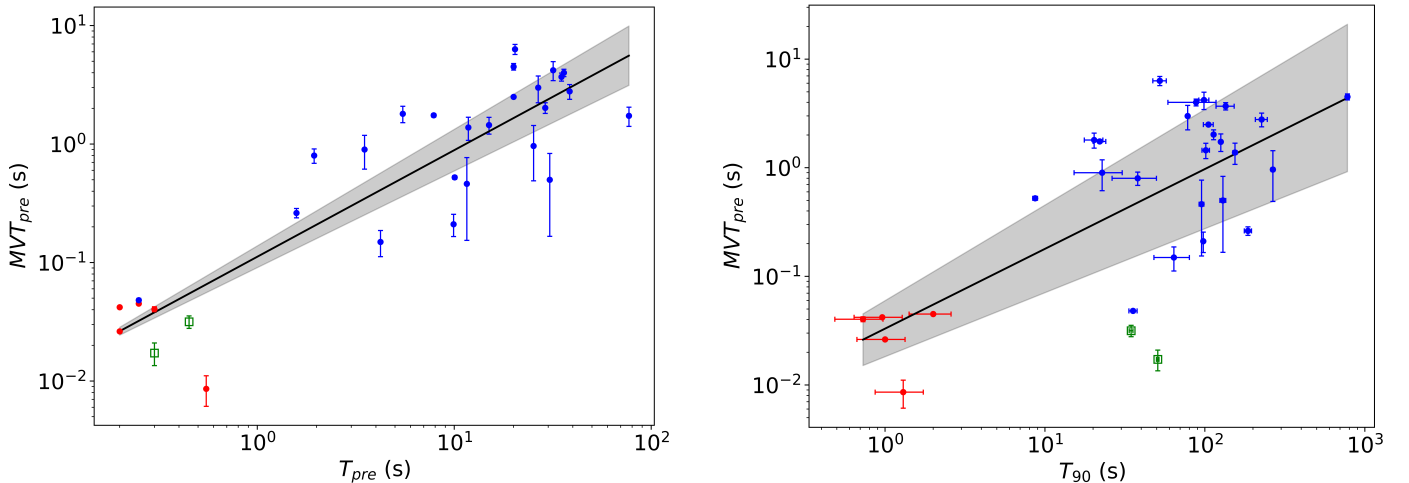


Fig. 10. Comparison of the minimum variability timescale MVT_{pre} of precursors, obtained from the sample of GRBs with precursors, against their corresponding T_{pre} (left) and T_{90} (right) durations. Precursor durations were collected from various sources, described in Section 3; however, uncertainties were not provided. In both plots, the long-duration burst grouped with the shorts and anomalies is GRB161129A. The slope of best fit is 0.90 ± 0.08 (left), and 0.75 ± 0.15 (right).

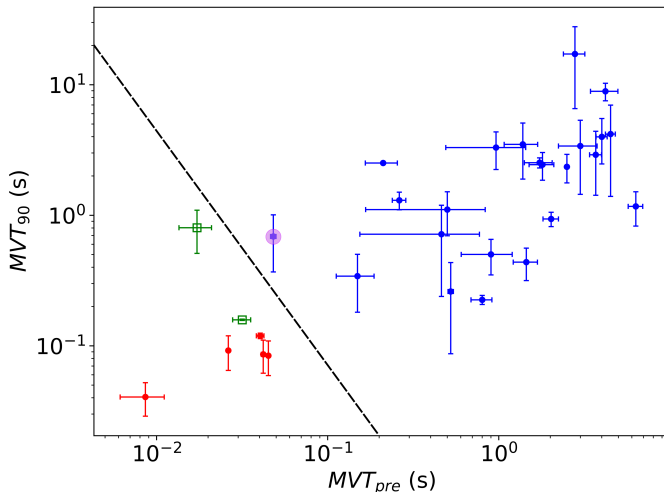


Fig. 11. Minimum variability timescale over the T_{90} duration, MVT_{90} , and precursor duration, MVT_{pre} . The dashed line is merely illustrative of a potential threshold to divide the domains of collapsar, and merger-originating GRBs, assuming that the enclosed point representing GRB161129A (highlighted in purple) is of collapsar origin.

bursts with a precursor MVT on the order of GRB161129A's remain duly sparse, then two further conclusions can be drawn. Contrary to this assumption one may consider that the separation observed thus far in Figures 10 and 11 between long and short duration bursts will become blurred as new data becomes available.

If the sparse GRBs, like GRB161129A, at the lower tail of the MVT_{pre} distribution predominately originate from collapsars, then Figure 10 alone will not be sufficient to differentiate them from CBMs. However, as Figure 11 demonstrates separation from believed CBM bursts, and GRB161129A, then we may define a rough domain (dashed-line) within this Figure 11 inside to which ownership predicates a high probability of merger origin. If instead, the source of sparse GRBs, like GRB161129A, is CBMs, then both Figures 10 and 11 would correctly observe clustering of these points with the remaining short and anomaly

CBM population. In such a case these plots may discern merger origin with an upper limit on the domain $MVT_{pre} < 10^{-1}$ s. In both cases, errors in these domains have not been calculated due to the paucity of data, and are only rough illustrations meant to be refined with the advent of new data. We also note that a linear boundary has been chosen for simplicity and may not encompass the full breadth of new data, despite aptly describing the samples used here.

6. Discussion

6.1. Sample size constraints

The aforementioned results have intentionally been presented in a reserved manner due to limitations of the sample size. While the number of long GRBs with a precursor or SN detection is rather small, this is accentuated in short-duration bursts. Coppin, Vries, and Eijndhoven (2020) find only 1.2% of short-duration *Fermi* bursts contain a precursor, and GRBs with an associated KN remain even more elusive with only a handful of observed events. Further, the low peak fluence and duration of short burst precursors poses challenges extracting a reliable MVT. From the five *Swift* precursors in the Troja, Rosswog, and Gehrels (2010) sample, only two meaningful MVT values could be identified. Equally scarce are the anomalous long-duration bursts with strong evidence of CBM origin, with only two of these (GRB211211A and GRB230307A) possessing a precursor. Therefore, while these initial results are very promising and correctly discern the anomalous GRBs, we again stress that they await further validation against a more expansive set of data. We also note that this method relies on the presence of a precursor, a feature that remains relatively rare.

6.2. Validity of findings

Here we explore the relationship between the MVT_{90} and MVT_{pre} in Figure 11. As previously noted, a correlation exists between T_{90} , T_{pre} and their respective MVT_{90} , MVT_{pre} , which we attributed partly to constraints on the MVT imposed by the

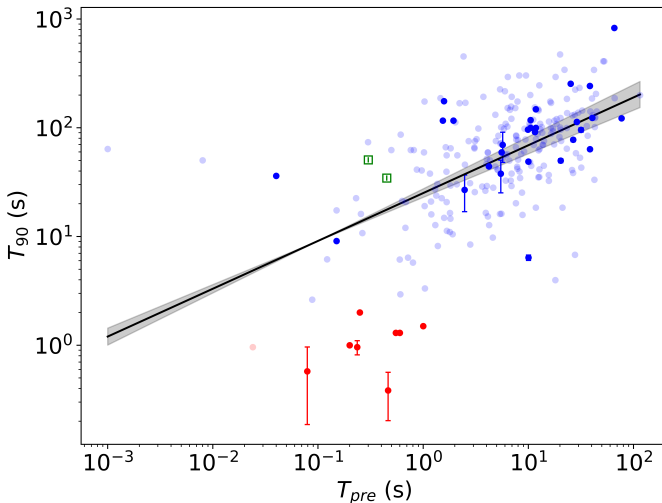


Fig. 12. Relationship between T_{90} and precursor duration T_{pre} , displaying two long-duration bursts (GRB090113, GRB161129A) analysed within our work (darker dots) with sub-1 s precursors. The lighter dots refer to the remaining 213 GRBs with precursors identified by Coppin, Vries, and Eijndhoven (2020). The slope of best-fit (inclusive of the lighter points) is described by 0.44 ± 0.04 .

duration. The correlation ($\rho = 0.78$, $p < 10^{-6}$) between MVT_{pre} and MVT_{90} shown in Figure 11, may therefore be the second order manifestation of these effects if the precursor and prompt duration are correlated. Additionally, the separation observed in MVT_{pre} between suspected CBMs and collapsars shown in Figure 10, could simply be a convoluted route to an underlying connection between precursor duration, T_{pre} , and progenitor source. This would still be a non-trivial finding but would necessarily bestow redundancy to the MVT analysis employed here, as a simpler measure of precursor duration could be used to discriminate the progenitor instead.

However, if the progenitor separation depicted in Figure 10 and 11 relies solely on temporal differences, as GRB211211A and GRB230307A were two of the brightest GRBs in recorded history, they have been analysed far more scrupulously than most GRBs. Compounded with the ensuing high flux and SNR, concern may arise that this would allow for the discrimination of short duration precursor flares that may potentially be missed by automated search methods. These methods often set a minimum signal threshold and separation from bulk emission on the order of 0.1 s (Coppin, Vries, and Eijndhoven, 2020). But as the duration between the precursor and prompt emission, termed the quiescent time, of GRB211211A and GRB230307A was approximately 1 s and 0.4 s, respectively, this substantially exceeds the threshold set by Coppin, Vries, and Eijndhoven (2020). These quiescent periods are typical (< 1.7 s) of other short GRBs within our sample. Furthermore, most precursor bursts within our sample are considerably fainter than those of the anomalous population, suggesting this is not an issue for precursor identification.

While a bias toward only very bright short-duration precursors, such as those of the anomalous group, is not problematic, a second concern arises that the clustering of the anomalous population with the short bursts in Figures 10 and 11 potentially stems from a small sample size of long-duration bursts with short precursors. To investigate this, we compared the pre-

sor duration to the T_{90} for the GRBs within our sample (dark dots), along with the remaining 213 *Fermi* precursors identified by Coppin, Vries, and Eijndhoven (2020) (light dots) in Figure 12. This reveals the existence of long GRBs with sub-1 s precursors, typical of short bursts, indicating that knowledge of only the T_{90} and T_{pre} is insufficient to resolve the anomalous population. Two long-duration bursts, GRB090113 and GRB161129A, analysed within our work meet this criteria of sub-1 s precursors. However, a reliable MVT for GRB090113 could not be identified as the precursor was far dimmer in the *Swift* LC analysed, compared to the *Fermi* detection documented. The remaining GRB161129A was found to cluster with the anomalous and short populations in Figure 10. Therefore, it is possible that the separation observed between progenitors in Figure 10, results from the lack of other long-duration bursts with short precursors. And given the numerous other long-duration GRBs with sub-1 s precursors within Figure 12, precursor duration may not correlate with the progenitor source. Addressing this concern requires further work analysing the MVT of the other long bursts with short precursors.

Figure 12 does, however, help elucidate the link between T_{90} and MVT_{pre} in Figure 10. A correlation ($\rho = 0.72$, $p = 6 \times 10^{-7}$) exists within our sample between the T_{90} and precursor duration. Therefore, given the connection between duration and MVT, and the correlation between the T_{90} and precursor duration, the T_{90} is thus partially linked to MVT_{pre} .

6.3. Understanding precursor dynamics

If precursor MVTs reliably differ between CBMs and collapsar GRBs, then several important consequences may follow. The first would support the notion of distinct mechanisms of precursor emission between progenitors, potentially lending credence to the RSF hypothesis in support of its theoretical inability to be replicated in collapsars. These unique mechanisms should produce physically distinct LCs that can be differentiated, at least in part, by analysing their MVT. However, due to the complexity of features the MVT depends upon, it is challenging to propose precisely what parameter changes. It is, of course, entirely possible that no one variable differs between the LCs in isolation. In such a case, the MVT analysis is well suited to disseminating this information, and as of yet, no simpler approach may exist. Unfortunately, this makes it difficult to draw any further conclusions about the underlying physical mechanism behind precursor flares.

If however, using the findings from Figure 5, we approximate that the MVT solely increases with a larger full width half maximum (FWHM) and, by extension, a smaller pulse amplitude. Then, since short-duration GRBs typically exhibit a lesser MVT_{pre} , we can infer that CBM precursors are generally shorter, more peaked, or possibly a combination of both. Figure 12 suggests that the relationship is not solely due to temporal differences; therefore, based on the prior assumption, it likely involves a combination of both a shorter and more peaked flare. We can test this hypothesis in a crude manner, evaluating the maximum count rate of precursors in the 1 ms LC, ensuring to only include *Swift* GRBs to maintain a similar photon detector sensitivity. From this simple analysis, Figure 13 shows T_{pre} against the precursor maximum peak flux A_{max} , illustrating that no such simple relationship exists between the progenitor and terse indicator of

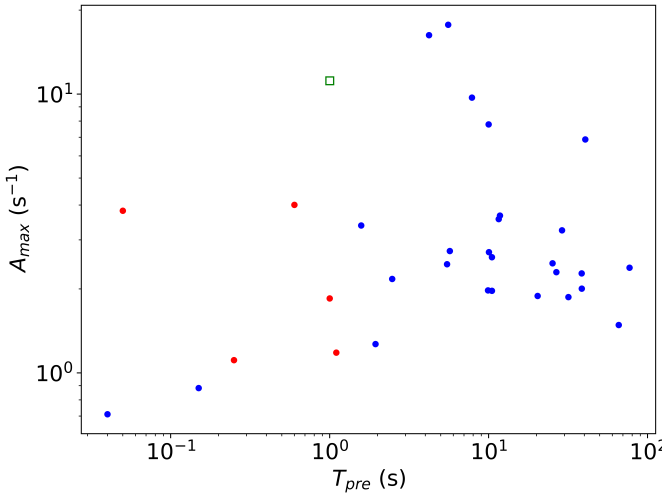


Fig. 13. Comparison between the *Swift* precursor duration T_{pre} and maximum amplitude A_{max} of the count rate over 1 ms binning.

FWHM. A similar dispersion of data is seen as one varies the bin size of the LC. Given such an unambiguous lack of correlation ($\rho = 0.08$, $p = 0.67$), it is unlikely that a more rigorous approach utilising Norris et al.’s (2005) four parameter FRED model to extract the amplitude, or FWHM directly, would yield a vastly different conclusion. This model would, however, much better handle the few precursors in the sample comprising of superimposing pulses, more reflective of the second simulated LC in Figure 4. In such a case, the amplitude derived would only be of the greatest flare but the duration would encapsulate the multiple flares within the precursor. Thus these measures would not reflect the FWHM of the shortest pulse, determined by Camisasca et al. (2023) to correlate with the MVT. Therefore based off Figure 13, the premise of this analysis is likely more complex, and we revert to our previous position of depicting the MVT as occupying a multi-faceted parameter space.

Another important finding is the incapacity of the minimum variable timescale, MVT_{90} , over the T_{90} to discern any meaningful difference between the anomalies and long-duration bursts. This is partially in contrast to Camisasca et al. (2023) who found that the FWHM of the shortest flare of anomalous GRBs was generally more appropriate of other short-duration bursts. As depicted above, we attribute this discrepancy between findings to the imperfect mapping between the MVT and FWHM. However, the domain occupied by these anomalous GRBs in Camisasca et al.’s (2023) figures of T_{90} against FWHM still greatly overlaps with a significant fraction of other long-duration bursts, thus failing to provide a distinct means of differentiation without additional evidence. In this regard, as both the bulk emission of CBMs and collapsars can be explained by the same fireball model, it may be the case that the domains of the parameters describing the LC are at least partially overlapping. One other particular variable we know this to be true for is the T_{90} , both in part to these anomalous GRBs as well as the intersecting T_{90} normal distributions of long and short bursts (assuming a symmetric distribution) (Veres et al., 2023). This suggests that while the FWHM and MVT_{90} analysis generally does a good job of separating long and short GRBs, we expect at least a partial overlap in the MVT_{90} of the two populations as observed in Figure 8.

6.4. Implications for the Fireball Model

Previous studies (Kocevski, Butler, and Bloom, 2007; Golkhou and Butler, 2014) have used the tenet that the MVT closely follows the rise time of the pulse to constrain the fireball model. We have seen how the observed rise time Δt_r of the pulse is governed by the width ΔR and Lorentz factor Γ of the merging shell in equation 1. In the source frame, however, we revert to the simpler expression,

$$\Delta R = c\Delta t_r. \quad (6)$$

If we assume that the particles initially ejected are confined within an optically thick fireball, and that their radius R_0 is comparable to that of the central engine, then as the material expands, the particles disperse outwards, forming an initial shell of thickness $\Delta R \sim R_0$. This occurs as the fireball becomes optically thin, allowing the particles within a radius $\sim R_0$ to escape, forming a shell of similar width. The shell further propagates and expands in thickness beyond R_0 . Therefore, when two such shells first collide, Equation 6 places an upper bound on the radius of the central engine, $\Delta R > R_0$. From the premise that the shortest observed rise time is equivalent to the MVT, Golkhou and Butler (2014) interchange the two terms to derive $R_0 < 3 \times 10^3$ km, using their smallest MVT_{90} value of 10 ms. From the same equivalence, they also imply a broad range of possible Lorentz factors, contrary to Walker, Schaefer, and Fenimore (2000). If we were to follow this logic, we find an identical minimum MVT_{90} of 10 ms for short-bursts, leading to a similar constraint on the size of the central engine of CBMs. For long-duration bursts, the smallest MVT_{90} is 130 ms, resulting in a slightly greater upper bound of $R_0 < 40 \times 10^3$ km for collapsar derived engines. However, in both instances we abstain from drawing this conclusion due to the lack of a simple connection found between the rise time and MVT. Importantly, we argue that the constraints imposed on the fireball model under the assumption that the MVT reflects the rise time are inaccurate.

7. Conclusion

We proposed an alternative and potentially less biased way to measure the MVT of GRBs LC by fitting a polynomial to the Allan variance $\sigma_{\Delta t}$ and measuring the first instant at which the rate of change is the greatest. We applied this method to three datasets comprising GRBs with precursors, supernova and kilonova, and mergers with anomalous T_{90} . From this, a rich distribution of MVT values over the T_{90} presents itself, ranging from 10 ms to 60 s. At the lower end of this domain we find exclusively short GRBs, and at the upper end purely long-duration bursts, with an overlapping region between 0.1 s and 0.3 s. Despite the strong separation, the anomalous GRBs remain invisible in the bulk of the long-duration cluster. This indistinguishably pertains when comparing this measure to the photon index.

Proceeding, we perform a novel analysis of the MVT over a relatively large sample of the available short and long *Swift* GRBs with precursors. From this, we find that short-duration bursts have a much smaller precursor MVT on average than their long-duration counterparts, and importantly, we find a strong coupling of the anomalous GRBs with the former. Therefore providing a way to potentially differentiate the two progenitor

sources where precursors are available. Following on from this, we propose the possibility that GRB161129A may also originate from a compact binary merger due to its substantially shorter precursor MVT. Finally, an analysis of a range of simulated pulses, indicates that previous connections between the MVT and the shortest observed rise time in the light curve may be unfounded. Importantly, this means that ensuing constraints on the fireball model may too be inaccurate.

While the method developed in this paper to determine the MVT allows for a fully automatic pipeline, the current approach relies on visually determining the best-fit polynomial degree. We note this to be the greatest hindrance of the method, and the dominant source of uncertainties. Therefore a major improvement would be to implement a reduced chi squared test to computationally determine this parameter. Despite this enhancement a significant drawback, not unique to our work, of variability analysis methodologies, is the frequency with which a clear rise phase in $\sigma_{\Delta t}$, and hence obvious MVT, evades. In the non-trivial number of GRBs this occurs in, it typically stems from oscillatory behaviour in $\sigma_{\Delta t}$. To overcome this, previous studies (Kocevski, Butler, and Bloom, 2007) have used a dyadic scale to increment Δt , or as we have done here, average $\sigma_{\Delta t}$ over growing bin widths to maintain a uniform dispersion in log space. The former merely samples the available domain, while the latter risks losing sensitivity at larger scales. In both instances, in GRBs with low SNR or multiple prominent pulses, the oscillatory behaviour may still prevail and perturb the rise phase. Further, extending the research conducted in Figure 5, we find at least a partial dependency of the MVT on the SNR. Future endeavours may therefore benefit from precisely determining the parameters we found to necessarily differ between precursors of CBMs and collapsars, if such simple measures exist. Conversely, as discussed in Section 6.3, matters may be more complex, and in such a case, the rich profiling of the MVT may be the best tool at hand.

A further improvement would involve evaluating the spectral hardness of the precursors in place of the photon index, as this method is far better suited to sparsely populated datasets with a low SNR.

Going forward, it would be of great interest to apply the techniques employed in this study to a more extensive selection of *Fermi* GRBs featuring precursors, considering that *Fermi* is more sensitive to a wider range of energies than *Swift*, so would generally include higher SNR LCs. Expanding the sample size beyond the scope of this study would not only serve to validate our findings but also explore the ability of the MVT analysis to differentiate short-duration collapsars. Furthermore, there is potential to extend this work by assessing the MVT across various γ -ray energy ranges, and even into the X-ray regime of the afterglow emission.

Despite these improvements, the early work analysing the MVT of precursors presented in this paper provides a promising avenue for discriminating the progenitor source of GRBs based on their γ -ray light curve alone.

8. Acknowledgements

I would like to thank Joel Fogarty for his extensive work in measuring the photon index of the sampled GRBs, and helping lay the groundwork for the code used to calculate the MVT.

Additionally, I express my gratitude to Patricia Schady for her continued support and guidance throughout the duration of the project, without which this paper wouldn't be possible.

References

- Abbott, Abbott, R., Abbott, T., Acernese, F., Ackley, K., Adams, C., Adams, T., Addesso, P., Adhikari, R., Adya, V., et al., 2017. Gravitational waves and gamma-rays from a binary neutron star merger: gw170817 and grb 170817a. *The astrophysical journal letters*, 848(2), p.L13.
- Allan, D.W., 1966. Statistics of atomic frequency standards. *Proceedings of the iee*, 54(2), pp.221–230.
- Barnacka, A. and Loeb, A., 2014. A size-duration trend for gamma-ray burst progenitors. *The astrophysical journal letters*, 794(1), p.L8.
- Beloborodov, A.M., Stern, B.E., and Svensson, R., 2000. Power density spectra of gamma-ray bursts. *The astrophysical journal*, 535(1), p.158.
- Caito, L., Bernardini, M.G., Bianco, C.L., Dainotti, M.G., Guida, R., and Ruffini, R., 2009. Grb060614: a “fake” short grb from a merging binary system. *Astronomy & astrophysics*, 498(2), pp.501–507.
- Camisasca, A., Guidorzi, C., Amati, L., Frontera, F., Song, X., Xiao, S., Xiong, S., Zhang, S., Margutti, R., Kobayashi, S., et al., 2023. Grb minimum variability timescale with insight-hxmt and swift-implications for progenitor models, dissipation physics, and grb classifications. *Astronomy & astrophysics*, 671, A112.
- Cano, Z., Malesani, Ugarte Postigo, A. de, Izzo, L., Thoene, C.C., and Castro-Rodriguez, N., 2021. *Gcn circular #20245*. Gamma-ray Coordinates Network Circular.
- Cano, Z., Wangand Dai, Z.-G., Wu, X.-F., et al., 2017. The observer’s guide to the gamma-ray burst supernova connection. *Advances in astronomy*, 2017.
- Coppin, P., Vries, K.D. de, and Eijndhoven, N. van, 2020. Identification of gamma-ray burst precursors in fermi-gbm bursts. *Physical review d*, 102(10), p.103014.
- D’Avanzo, P., 2015. Short gamma-ray bursts: a review. *Journal of high energy astrophysics*, 7, pp.73–80.
- Daigne, F. and Mochkovitch, R., 2003. The physics of pulses in gamma-ray bursts: emission processes, temporal profiles and time-lags. *Monthly notices of the royal astronomical society*, 342(2), pp.587–592.
- Dichiara, S., Tsang, D., Troja, E., Neill, D., Norris, J., and Yang, Y.-H., 2023. A luminous precursor in the extremely bright grb 230307a. *The astrophysical journal letters*, 954(1), p.L29.
- Ferro, M., Brivio, R., D’Avanzo, P., Rossi, A., Izzo, L., Campana, S., Christensen, L., Dinatolo, M., Hussein, S., Levan, et al., 2023. A search for the afterglows, kilonovae, and host galaxies of two short grbs: grb 211106a and grb 211227a. *Astronomy & astrophysics*, 678, A142.

- Ghirlanda, G., Nava, L., Ghisellini, G., Celotti, A., and Firmani, C., 2009. Short versus long gamma-ray bursts: spectra, energetics, and luminosities. *Astronomy & astrophysics*, 496(3), pp.585–595.
- Golkhou, V.Z., Butler, and Littlejohns, O.M., 2015. The energy dependence of grb minimum variability timescales. *The astrophysical journal*, 811(2), p.93.
- Golkhou, V.Z. and Butler, 2014. Uncovering the intrinsic variability of gamma-ray bursts. *The astrophysical journal*, 787(1), p.90.
- Gompertz, O'Brien, P., Wynn, G., and Rowlinson, A., 2013. Can magnetar spin-down power extended emission in some short grbs? *Monthly notices of the royal astronomical society*, 431(2), pp.1745–1751.
- Heintz, K.E., Malesani, D., Cano, Z., De Ugarte Postigo, A., Fedorets, G., Tronsgaard Rasmussen, R., Djupvik, A.A., Losada, I.R., Svardh, I., Clasen, J., and Armas Perez, S., 2021. *Gcn circular #20244*. Gamma-ray Coordinates Network Circular.
- Hughes, P., Aller, and Aller, 1992. The university of michigan radio astronomy data base. i-structure function analysis and the relation between bl lacertae objects and quasi-stellar objects. *Astrophysical journal, part 1 (issn 0004-637x)*, vol. 396, no. 2, sept. 10, 1992, p. 469-486., 396, pp.469–486.
- Klebesadel, R.W., Strong, I.B., and Olson, R.A., 1973. Observations of gamma-ray bursts of cosmic origin. *Astrophysical journal*, vol. 182, p. l85, 182, p.L85.
- Kocevski, D., Butler, and Bloom, J.S., 2007. Pulse width evolution of late-time x-ray flares in gamma-ray bursts. *The astrophysical journal*, 667(2), p.1024.
- Kolaczyk, E.D., 1997. Nonparametric estimation of gamma-ray burst intensities using haar wavelets. *The astrophysical journal*, 483(1), p.340.
- Kouveliotou, C., Meegan, C.A., Fishman, G.J., Bhat, N.P., Briggs, M.S., Koshut, T.M., Paciesas, W.S., and Pendleton, G.N., 1993. Identification of Two Classes of Gamma-Ray Bursts. *Apj [Online]*, 413 (), p.L101. Available from: <https://doi.org/10.1086/186969>.
- Kulkarni, S., Frail, D., Sari, R., Moriarty-Schieven, G., Shepherd, D., Udomprasert, P., Readhead, A., Bloom, J., Feroci, M., and Costa, E., 1999. Discovery of a radio flare from grb 990123. *The astrophysical journal*, 522(2), p.L97.
- Kumar, P. and Zhang, 2015. The physics of gamma-ray bursts & relativistic jets. *Physics reports*, 561, pp.1–109.
- Lazzati, D., 2005. Precursor activity in bright, long batse gamma-ray bursts. *Monthly notices of the royal astronomical society*, 357(2), pp.722–731.
- Levan, A.J., Gompertz, B., Salafia, O.S., Bulla, M., Burns, E., Hotokezaka, K., Izzo, L., Lamb, G.P., Malesani, D.B., Oates, S.R., et al., 2023. Heavy-element production in a compact object merger observed by jwst. *Nature*, pp.1–5.
- Link, B., Epstein, R.I., and Priedhorsky, W.C., 1993. Prevalent properties of gamma-ray burst variability. *Astrophysical journal, part 2-letters (issn 0004-637x)*, vol. 408, no. 2, p. 181-184., 408, pp.L81–L84.
- Lü, H.-J., Yuan, H.-Y., Yi, T.-F., Wang, X.-G., Hu, Y.-D., Yuan, Y., Rice, J., Wang, J.-G., Cao, J.-X., Kong, D.-F., et al., 2022. Grb 211227a as a peculiar long gamma-ray burst from a compact star merger. *The astrophysical journal letters*, 931(2), p.L23.
- MacLachlan, G., Shenoy, A., Sonbas, E., Dhuga, K.S., Cobb, B.E., Ukwatta, T., Morris, D.C., Eskandarian, A., Maximon, L., and Parke, W.C., 2013. Minimum variability time-scales of long and short grbs. *Monthly notices of the royal astronomical society*, 432(2), pp.857–865.
- Matsumoto, T. and Piran, T., 2020. On short grbs similar to grb 170817a detected by fermi-gbm. *Monthly notices of the royal astronomical society*, 492(3), pp.4283–4290.
- Mészáros, P. and Rees, M., 1994. Delayed gev emission from cosmological gamma-ray bursts: impact of a relativistic wind on external matter. *Monthly notices of the royal astronomical society*, 269(1), pp.L41–L43.
- Mészáros, P. and Rees, M., 1999. Grb 990123: reverse and internal shock flashes and late afterglow behaviour. *Monthly notices of the royal astronomical society*, 306(3), pp.L39–L43.
- Murakami, T., Inoue, H., Nishimura, J., Van Paradijs, J., Fenimore, E., Ulmer, A., and Yoshida, A., 1991. A γ -ray burst preceded by x-ray activity. *Nature*, 350(6319), pp.592–594.
- Nakar, E., 2007. Short-hard gamma-ray bursts. *Physics reports*, 442(1-6), pp.166–236.
- Neill, D., Tsang, D., Van Eerten, H., Ryan, G., and Newton, W.G., 2022. Resonant shattering flares in black hole-neutron star and binary neutron star mergers. *Monthly notices of the royal astronomical society*, 514(4), pp.5385–5402.
- Norris, J.P., Bonnell, J.T., Kazanas, D., Scargle, J.D., Hakkila, J., and Giblin, T.W., 2005. Long-lag, wide-pulse gamma-ray bursts. *The astrophysical journal*, 627(1), p.324.
- Pe'Er, A. et al., 2015. Physics of gamma-ray bursts prompt emission. *Advances in astronomy*, 2015.
- Piran, T., 2005. The physics of gamma-ray bursts. *Reviews of modern physics*, 76(4), p.1143.
- Piran, T., Narayan, R., et al., 1998. Spectra and light curves of gamma-ray burst afterglows. *The astrophysical journal*, 497(1), p.L17.
- Ramirez-Ruiz, E., MacFadyen, A.I., and Lazzati, D., 2002. Precursors and e \pm pair loading from erupting fireballs. *Monthly notices of the royal astronomical society*, 331(1), pp.197–202.
- Rastinejad, J.C., Gompertz, B.P., Levan, A.J., Fong, W.-f., Nicholl, M., Lamb, G.P., Malesani, D.B., Nugent, A.E., Oates, S., Tanvir, N., et al., 2022. A kilonova following a long-duration gamma-ray burst at 350 mpc. *Nature*, 612(7939), pp.223–227.

Tanvir, N., Levan, A.J., Fruchter, A., Hjorth, J., Hounsell, R., Wiersema, K., and Tunnicliffe, R., 2013. A ‘kilonova’ associated with the short-duration γ -ray burst grb 130603b. *Nature*, 500(7464), pp.547–549.

Tarnopolski, M., 2019. Analysis of the duration–hardness ratio plane of gamma-ray bursts using skewed distributions. *The astrophysical journal*, 870(2), p.105.

Trevese, D., Kron, R.G., Majewski, S.R., Bershadsky, M.A., and Koo, D.C., 1994. The ensemble variability properties of faint qsos. *Arxiv preprint astro-ph/9407003*.

Troja, E., Castro-Tirado, A.J., Becerra González, J., Hu, Y., Ryan, G., Cenko, S., Ricci, R., Novara, G., Sánchez-Rámirez, R., Acosta-Pulido, J., et al., 2019. The afterglow and kilonova of the short grb 160821b. *Monthly notices of the royal astronomical society*, 489(2), pp.2104–2116.

Troja, E., Rosswog, S., and Gehrels, N., 2010. Precursors of short gamma-ray bursts. *The astrophysical journal*, 723(2), p.1711.

Veres, P., Bhat, P., Burns, E., Hamburg, R., Fraija, N., Kocevski, D., Preece, R., Poolakkil, S., Christensen, N., Bizouard, M., et al., 2023. Extreme variability in a long-duration gamma-ray burst associated with a kilonova. *The astrophysical journal letters*, 954(1), p.L5.

Von Kienlin, A., Meegan, C., Paciesas, W., Bhat, P., Bissaldi, E., Briggs, M., Burns, E., Cleveland, W., Gibby, M., Giles, M., et al., 2020. The fourth fermi-gbm gamma-ray burst catalog: a decade of data. *The astrophysical journal*, 893(1), p.46.

Walker, K.C., Schaefer, B.E., and Fenimore, E., 2000. Gamma-ray bursts have millisecond variability. *The astrophysical journal*, 537(1), p.264.

Yang, B., Jin, Z.-P., Li, X., Covino, S., Zheng, X.-Z., Hotokezaka, K., Fan, Y.-Z., Piran, T., and Wei, D.-M., 2015. A possible macronova in the late afterglow of the long–short burst grb 060614. *Nature communications*, 6(1), p.7323.

Zhong, S.-Q., Dai, Z.-G., Cheng, J.-G., Lan, L., and Zhang, H.-M., 2019. Precursors in short gamma-ray bursts as a possible probe of progenitors. *The astrophysical journal*, 884(1), p.25.

Zhou, Gao, Y., Zhou, Y., Lai, X., Shao, L., Wang, W., Xiong, S., Xu, R., Yi, S., Yim, G., et al., 2024. The precursor of grb211211a: a tide-induced giant quake? *Research in astronomy and astrophysics*.

Appendix A: Gamma-ray light curves of the anomalous GRBs

Fig. A.1. The γ -ray light curve of GRB060614 (top), GRB211211A (second), GRB211227A (third), and GRB230307A (bottom), with delineations marking the T_{90} (green dashed lines) and precursor duration (red dashed lines) at a binning of 64 ms.

